

Contamination of the Central Sunyaev–Zel’dovich Decrements in AMiBA Galaxy Cluster Observations

Guo-Chin Liu^{1,2}, Mark Birkinshaw³, Jiun-Huei Protty Wu⁵, Paul T. P. Ho^{1,4} Chih-Wei Locutus Huang⁵, Yu-Wei Liao⁵, Kai-Yang Lin^{1,5}, Sandor M. Molnar¹, Hiroaki Nishioka¹, Patrick M. Koch¹, Keiichi Umetsu¹, Fu-Cheng Wang⁵, Pablo Altamirano¹, Chia-Hao Chang¹, Shu-Hao Chang¹, Su-Wei Chang¹, Ming-Tang Chen¹, Chih-Chiang Han¹, Yau-De Huang¹, Yuh-Jing Hwang¹, Homin Jiang¹, Michael Kesteven⁶, Derek Kubo¹, Chao-Te Li¹, Pierre Martin-Cocher¹, Peter Oshiro¹, Philippe Raffin¹, Tashun Wei¹, Warwick Wilson⁶

Received _____; accepted _____

submitted to ApJ

¹Academia Sinica, Institute of Astronomy and Astrophysics, P.O.Box 23-141, Taipei 106, Taiwan

²Department of Physics, Tamkang University, 251-37 Tamsui, Taipei County, Taiwan

³Department of Physics, University of Bristol, Tyndall Ave, Bristol, BS8 1TL, UK

⁴Harvard-Smithsonian Center for Astrophysics, 60 Garden Street, Cambridge, MA 02138, USA

⁵Department of Physics, Institute of Astrophysics, & Center for Theoretical Sciences, National Taiwan University, Taipei 10617, Taiwan

⁶Australia Telescope National Facility, P.O.Box 76, Epping NSW 1710, Australia

ABSTRACT

We investigate the contamination of the Sunyaev–Zel’dovich (SZ) effect for six galaxy clusters, A1689, A1995, A2142, A2163, A2261, and A2390, observed by the Y. T. Lee Array for Microwave Background Anisotropy during 2007. With the range of baselines used, we find that the largest effect (of order 13% – 50% of the central SZ flux density) comes from primary anisotropies in the cosmic microwave background and exceeds the thermal noise in all six cases. Contamination from discrete radio sources is estimated to be at a level of (3% – 60%) of the central SZ flux density. We use the statistics of these contaminating sources to estimate and correct the errors in the measured SZ effects of these clusters.

Subject headings: cosmic background radiation - cosmology: observations – diffuse radiation- galaxy clusters: general

1. Introduction

Measurements of the Sunyaev-Zel’dovich effect (Sunyaev & Zel’dovich 1972, SZE) are contaminated by foregrounds and backgrounds at a level that depends on the angular scale of interest and the frequency of observation. Primary anisotropies in the cosmic microwave background (CMB) from redshift $z \simeq 1100$ dominate on scales larger than a few arcminutes ($\ell \lesssim 2000$) but have a spectrum that differs significantly from the SZE, and so can be removed by multiwavelength observations. Galactic contamination arises from synchrotron, free-free, and dust emission and can also affect SZE measurements. Synchrotron and free-free emission usually dominate at low radio frequencies, while dust emission is most important at millimeter and submillimeter wavelengths, with a crossover frequency of 60 – 70 GHz. Emission from discrete radio sources is less important at high radio frequencies, but can be problematic even at 90 GHz. Spatial filtering, by observing at a finer angular resolution than the scale of the SZE, can mitigate this problem. Finally, SZE data are commonly affected by the pickup of signals from the ground, the atmosphere, and other local emitters, which have to be carefully corrected for or avoided.

Array for Microwave Background Anisotropy (AMiBA; Ho et al. 2009; Chen et al. 2009; Koch et al. 2009a; Wu et al. 2009; Li et al. 2010) will be subject to all these issues. AMiBA was designed to operate from 86 to 102 GHz and to be sensitive to multipoles $800 \lesssim \ell \lesssim 2600$ with the initial close-packed configuration of seven 0.6m antennas (see Figure 2 of Ho et al. 2009), and to $1600 \lesssim \ell \lesssim 9000$ with the current upgraded configuration of thirteen 1.2m antennas (Molnar et al. 2010).

The observing frequency was chosen to minimize contamination from non-SZE while working within a window of good atmospheric transmission. It is generally assumed that radio source contamination is less of a problem for AMiBA than for other instruments that operate at lower frequencies. However, sources with inverted spectra may still cause

difficulties, so it is important to consider the radio environment for any AMiBA field. The level of CMB contamination may be anomalously high in any particular field, and this should also be investigated. The purpose of this paper is to investigate, and correct for, these contaminations in the SZE signals measured from the first-year AMiBA observation, so as to provide unbiased SZE estimations for further science investigations in our companion papers.

We do not, here, consider the effects of ground pick-up and other technical issues to do with the observing technique — the two-patch method used to deal with such problems is discussed elsewhere (Lin et al. 2009, Wu et al. 2009). Rather we investigate the CMB and Galactic emission environment (using data from the *Wilkinson Microwave Anisotropy Probe*, *WMAP*) and the known centimeter-wave radio source population (using source lists from several surveys) to estimate their effect on SZE results for the six clusters of galaxies observed by AMiBA. We describe our SZE analysis in Section 2, and discuss the errors in the presence of the sources of contamination in Section 3. A summary of the final results is given in Section 4.

2. SZE Flux Analysis

Between 2007 April and August AMiBA observed six galaxy clusters, A1689, A1995, A2142, A2163, A2261 and A2390. These SZE data have been combined with X-ray information in the literature to estimate the Hubble constant (Koch et al. 2009b) and study the scaling relation (Huang et al. 2009, Liao et al. 2010). In combination with Subaru weak lensing data they have also been used to study the gas fraction (Umetsu et al. 2009). Crucial to this work is the proper estimation of the errors on the measured SZE in the presence of contaminating signals. In this section we describe the basic analysis used to measure the key parameters of the cluster SZE.

The fundamental observable for AMiBA is the visibility, which is the Fourier transform of the sky intensity multiplied by the primary beam or aperture function:

$$\mathcal{V}(u, v) = g \int dx dy A(x, y) \Delta I(x, y) e^{-2\pi i(ux+vy)}, \quad (1)$$

where g is a gain factor, which can be measured by calibration, (u, v) are components of the spatial separation vector of two antennas in the array in units of the observing wavelength, λ , $A(x, y)$ is the primary beam pattern, (x, y) are two components of angular position on the sky, measured relative to the phase center (taken here to coincide with the pointing center), and $\Delta I(x, y)$ is the distribution of surface brightness of the sky. Here we have approximated the sky as being flat. Details of the conversion from correlator data to visibilities are described in Wu et al. (2009).

Given the SZE flux density in the sky, one can calculate the visibility from Equation (1). The SZE flux density of a cluster depends on observing frequency, the physics of the cluster atmosphere (gas temperature and density distributions, peculiar velocity, etc), and the angular diameter distance, D_A . If we adopt a spherical isothermal β -model (Cavaliere & Fusco-Femiano 1976), the visibilities measured by an interferometer are

$$\begin{aligned} \mathcal{V}_{\text{SZE}}(u, v) = I_0 \int dx dy A(x, y) & \left(1 + \frac{\theta^2}{\theta_0^2}\right)^{-\frac{3}{2}\beta + \frac{1}{2}} \\ & \times e^{-2\pi i(ux+vy)}, \end{aligned} \quad (2)$$

where I_0 is the central surface brightness of the SZE, $\theta^2 = (x - x_0)^2 + (y - y_0)^2$, (x_0, y_0) gives the sky position of the center of the cluster, θ_0 is the angular core radius of the cluster, and β is the shape parameter.

For much of the SZE science (Birkinshaw 1999) that we can currently tackle with AMiBA we need to estimate the quantity I_0 by fitting the model in Equation (2) to the measured visibilities. AMiBA visibilities are estimated in a process that includes conversion

from the wide-band, 4-lag, correlated analog signal into visibilities in two frequency channels (Wu et al. 2009) after tests on the quality of the data as discussed by Nishioka et al. (2009). In the hexagonal close-packed configuration used for observing the six clusters, the seven elements instantaneously yield 21 baseline vectors of three different lengths. Eight platform rotation angles relative to the pointing center are used to improve the $u - v$ sampling.

In Figure 1, we show the observed real and imaginary parts of the visibilities as a function of multipole $\ell = 2\pi(u^2 + v^2)^{1/2}$. The averaging in azimuth uses σ^{-2} noise weighting, and for each baseline length the information from the two frequency channels is combined.

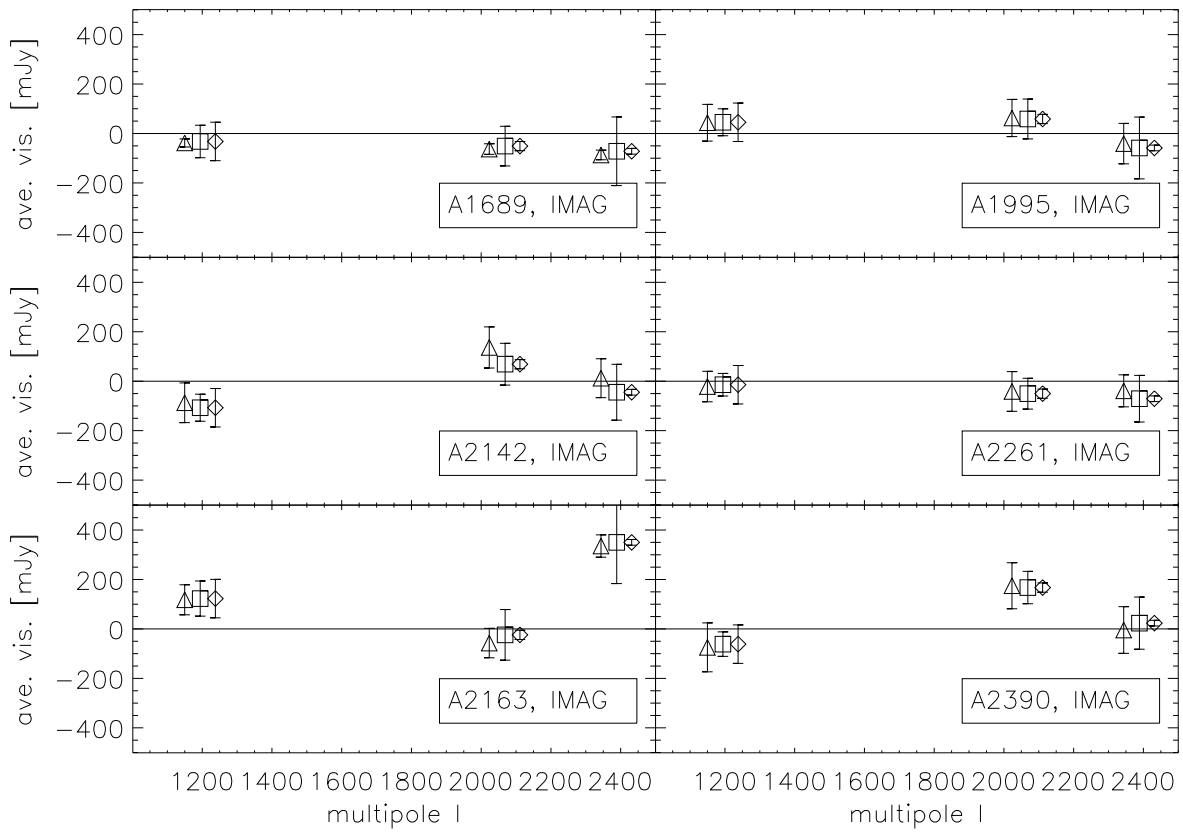
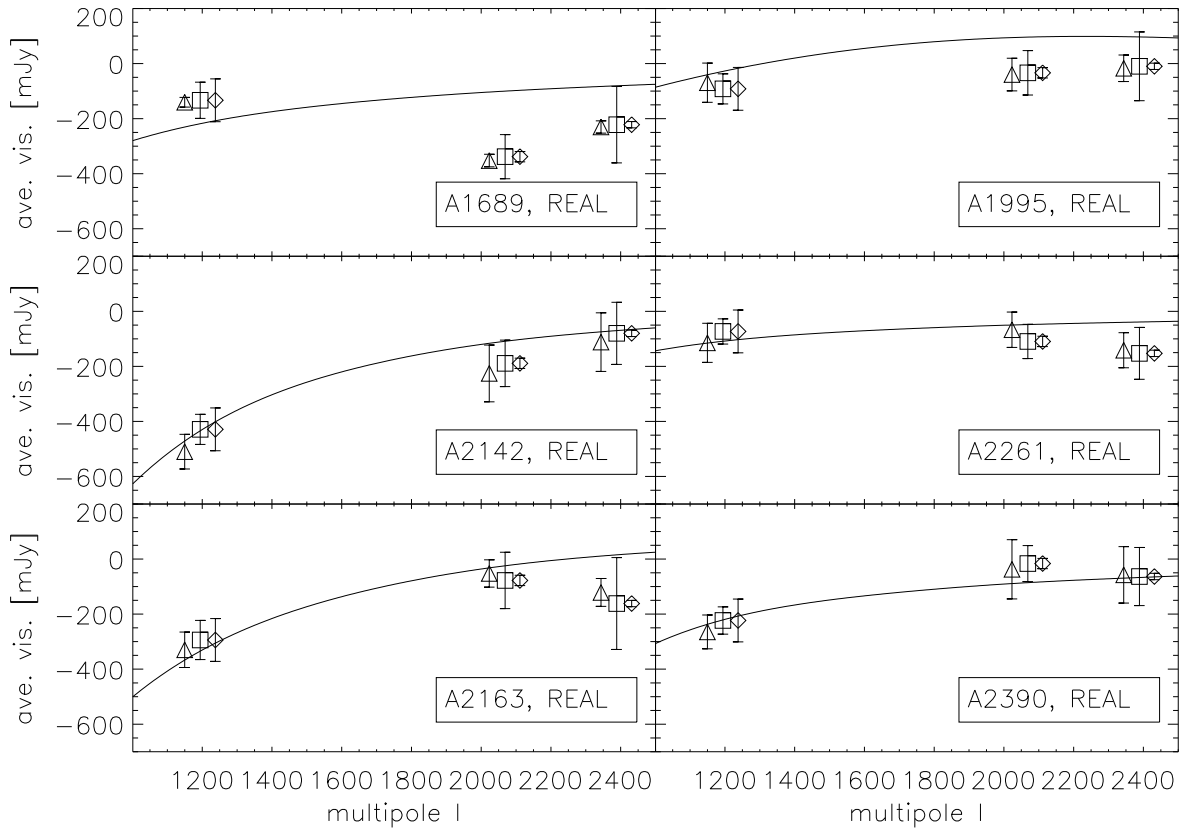
We fit the visibility model in Equation (2) by minimizing χ^2 with respect to I_0 and the location (x_0, y_0) of the cluster center. Because of the limited coverage in ℓ , the values of β and θ_0 can not be usefully constrained by our data so we use values from the literature, which are consistently used by our companion papers (Huang et al. 2009, Koch et al. 2009b, Wu et al. 2009).

The fitted results for I_0 , x_0 , and y_0 for the clusters are given in Table 1. The errors were calculated from the Hessian matrix in the usual manner. The best-fit visibility profiles are shown with the data in Figure 1. At this stage no contribution to the errors from CMB or radio source confusion has been taken into account. These effects are the subject of the remainder of this paper.

3. Error Analysis

3.1. Large-scale CMB and Galactic-emission contamination

WMAP has recently released full-sky temperature and polarization maps based on their five-year accumulated data. The angular resolution of *WMAP* varies from $0^\circ.88$ to



$0^\circ.22$ over five bands from 23 to 94 GHz, and since the frequency range extends up to the AMiBA operating band, the *WMAP* data provide a good check on the level of CMB and Galactic contamination of the AMiBA data, although at lower angular resolution.

We use the CMB map produced by the internal linear combination (ILC) method that is independent of both external data and assumptions about foreground emission, and estimate the Galactic foreground using the maps of synchrotron, free-free, and dust foregrounds produced by the maximum entropy method (Gold et al. 2008). All four maps are smoothed to 1° scales, so that the principal indication that can be obtained is only whether there are unusually “hot” or “cold” spots near the clusters or trailing fields, and so whether there is likely to be additional noise power on the angular scales to which AMiBA is sensitive.

We find no strong Galactic contamination in any of the six clusters, with the total Galactic emission being typically an order of magnitude fainter than the CMB signal (Table 2). On the smaller angular scales to which AMiBA is sensitive, the Galactic emission will be even less important, since its power spectrum falls roughly as a power law, $C_\ell \propto \ell^{-\gamma}$, with $\gamma = 2.0 - 3.0$ (Tegmark et al. 2000). Here the power spectrum is defined as

$$C_\ell = \frac{1}{2\ell + 1} \sum_m \langle a_{\ell m}^* a_{\ell m} \rangle \quad (3)$$

with $a_{\ell m}$ being the expansion coefficient of the temperature field on the spherical harmonics. Thus, we expect that Galactic contamination will be two orders of magnitude fainter than the primordial CMB signal as seen in the *WMAP* data.

We summarize the CMB surface brightness fluctuations in the clusters and trailing fields on the angular scale of the clusters, based on the *WMAP* ILC image, in Table 2. The values range up to ~ 25 kJy sr $^{-1}$ (~ 100 μ K in temperature units). The level of primordial contamination at the degree scale in our data is suppressed by the 45 arcmin separated two-patch subtraction technique that we use, but nevertheless we might expect elevated

levels of CMB noise in fields with large degree-scale signals. This is consistent with the observed deviations from the expected visibility curves for the most contaminated clusters, A1689 and A2390.

3.2. Small-scale CMB and Galactic-emission estimation

Given the statistical properties of the CMB and Galactic emission, we are able to estimate the rms fluctuations on each baseline. Because of the two-patch observing strategy, we rewrite Equation (1) as

$$\begin{aligned}
 \mathcal{V}(u_j, v_j, x_p, y_p) &= \int dx dy A(x - x_p, y - y_p) \Delta I(x, y) \\
 &\quad \times e^{-2\pi i(u_j(x-x_p) + v_j(y-y_p))} \\
 &= \int dudv \tilde{A}(u_j - u, v_j - v) a(u, v) \\
 &\quad \times e^{2\pi i(ux_p + vy_p)},
 \end{aligned} \tag{4}$$

where (x_p, y_p) is the pointing center of the corresponding field, and $a(u, v)$ is the Fourier transform of surface brightness of the sky. The two-point correlation function of $a(\mathbf{u})$ is diagonal because of the rotation invariant

$$\langle a(\mathbf{u})a(\mathbf{w}) \rangle = C_{\mathbf{u}} \delta^{(2)}(\mathbf{u} - \mathbf{w}), \tag{5}$$

where $C_{\mathbf{u}} = (\partial B_\nu / \partial T)^2 C_\ell$ and $\partial B_\nu / \partial T$ converts from temperature to intensity. We have adopted the flat-sky approximation, which is valid for AMiBA, so that $\ell = 2\pi \mathbf{u} = 2\pi \sqrt{u^2 + v^2}$.

The rms fluctuation in each baseline is then

$$\begin{aligned}
 \langle \mathcal{V}^2(u_j, v_j) \rangle &= \int du dv \quad \tilde{A}^2(u_j - u, v_j - v) C_\ell \\
 &\quad \times (1 - \cos[2\pi(u\Delta x + v\Delta y)]) \quad ,
 \end{aligned} \tag{6}$$

Table 1. Best-fit Values for I_0 and Offset of the Cluster centres, with $1\text{-}\sigma$ Uncertainties Ignoring the Effects of Contamination.

Cluster	I_0 ($\times 10^5 \text{ Jy sr}^{-1}$)	Offset in R.A. (arcmin)	Offset in Decl. (arcmin)
A1689	-2.24 ± 0.44	-0.05 ± 0.63	0.02 ± 0.63
A1995	-3.38 ± 0.63	4.41 ± 0.76	0.38 ± 0.68
A2142	-2.16 ± 0.19	-0.64 ± 0.42	0.19 ± 0.41
A2163	-3.56 ± 0.37	2.53 ± 0.47	-2.36 ± 0.53
A2261	-1.46 ± 0.40	0.43 ± 1.21	1.31 ± 1.19
A2390	-2.42 ± 0.36	0.60 ± 0.81	-1.74 ± 0.56

Table 2. Large-scale CMB and Galactic Emission (Smoothed to 1° Scales).

Cluster	CMB(lead;trail) ($\times 10^3 \text{ Jy sr}^{-1}$)	Galactic(lead;trail) ($\times 10^3 \text{ Jy sr}^{-1}$)
A1689	+24.1; +22.3	0.0; 0.0
A1995	- 5.6; +14.0	0.0; 0.0
A2142	+ 8.5; +14.8	0.0; 0.0
A2163	+17.2; - 4.3	1.1; 7.3
A2261	- 0.2; + 4.2	0.5; 0.4
A2390	-25.2; -20.7	4.0; 1.4

where \tilde{A} is the Fourier transform of the primary beam, $(\Delta x, \Delta y)$ is the separation of the clusters and trailing fields (about 45 arcmin in most of our data). Since the universe is isotropic, we put $\Delta x = 45$ and $\Delta y = 0$ arcmin when we calculate the rms fluctuation. The $1\text{-}\sigma$ uncertainties caused by the CMB at the l ranges corresponding to AMiBA baselines are plotted in Figure 1 as shown by the diamond symbol.

For the Galactic emission, we use the middle-of-the-road (MID) foreground model in Tegmark et al. (2000), which is intended to be realistic but conservative. We show the expected fluctuation from three Galactic emission components in Figure 2. The Galactic emission lies about two orders of magnitude below the contribution from the CMB. Other models in Tegmark et al. (2000) change the results by less than a factor of 2. These results are consistent with what we estimated in Section 3.1. Therefore, we ignore the contribution from Galactic emission in what follows.

The CMB surface brightness fluctuations expected for a Λ CDM model with cosmological parameters as estimated from the *WMAP* five-year data alone (Dunkley et al. 2009) contribute uncertainties of 80.6, 20, and 11.4 mJy for the three averaged AMiBA baselines and exceed the instrument noise for all baselines in all six clusters.

To estimate the error in I_0 from CMB anisotropies, we repeat the fitting of Section. 2 for 500 simulated CMB skies where the CMB anisotropies have a power spectrum based on the cosmological parameters from the five-year *WMAP* data. For each simulation we subtract the simulated CMB visibilities from the data and fit I_0 , assuming that the central positions in Table 1 are unchanged. Our results for the noise introduced in the values of I_0 , σ_{CMB} , are given in Table 3.

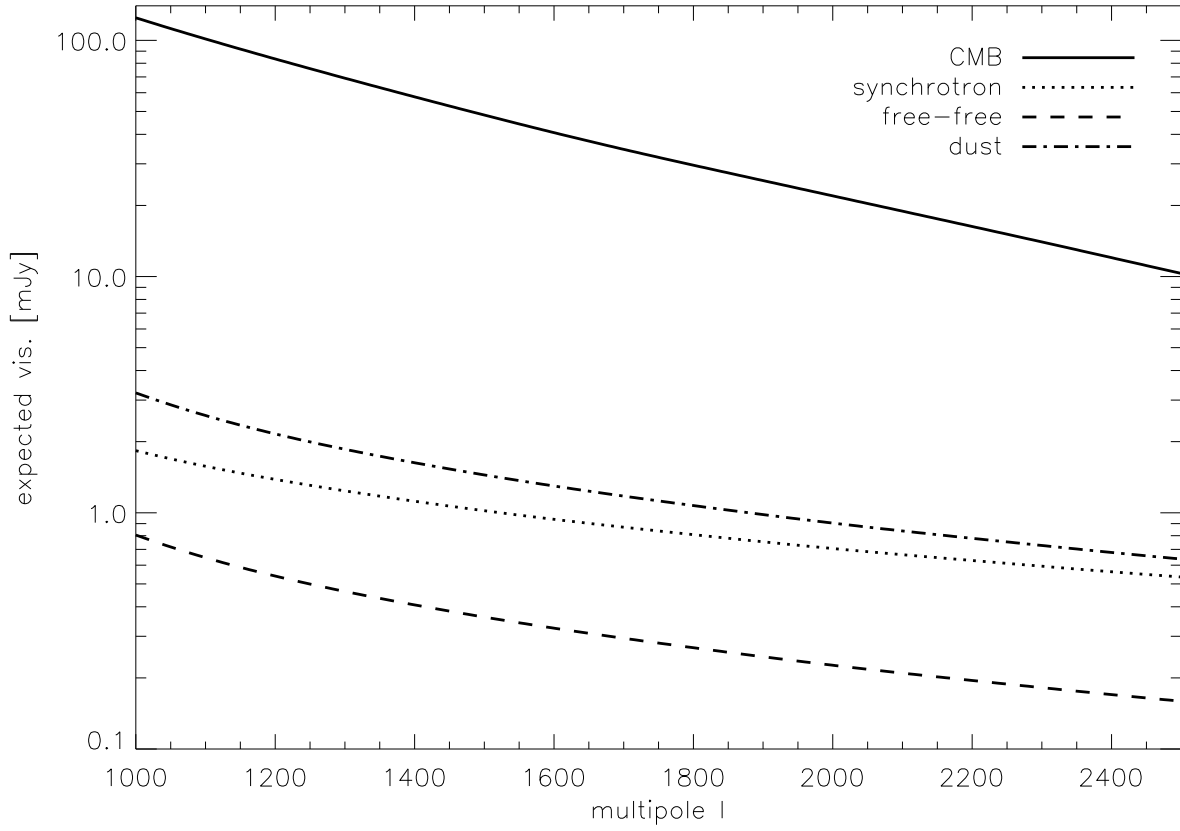


Fig. 2.— Expected response from CMB (solid line), synchrotron (dotted line), free-free (dashed line), and dust (dot-dashed) emission as a function of multipole ℓ .

3.3. Foreground Point Sources

The emission from discrete sources will reduce the size of the SZE at 94 GHz if those sources are concentrated towards the target cluster, but can cause an increase in the measured value of I_0 if they are located in the trailing field (or lie in negative sidelobes of the synthesized beam). Since we expect to see more radio sources toward the clusters, the measured SZE will normally be an underestimate of the true value (Coble et al. 2007).

Corrections for point source contamination can often be made by combining arcminute-resolution SZE data with high-resolution data (see, e.g., Lancaster et al. 2005; Udomprasert et al. 2004). However, such supporting data are not available for AMiBA. Because the point source population at 90 GHz is also poorly known, it is challenging to estimate the degree of contamination. Thus, we take the following approach.

In assessing the contributions from known sources, we use the 4.85 GHz GB6 and PMN catalogs (Gregory et al. 1996; Griffith et al. 1995). The GB6 survey covered declinations $0^\circ < \delta < +75^\circ$ to a flux density limit $S_{4.85} = 18$ mJy. The four declination bands in the PMN survey from $-88^\circ < \delta < +10^\circ$ and have flux density limits $S_{4.85} = 20 - 70$ mJy. We estimate the contamination for fainter sources with significant low-frequency emission using the NVSS catalog at 1.4 GHz (Condon et al. 1998), which is complete for $\delta > -40^\circ$ with flux density limit 2.5 mJy. In each case, we investigate the radio environments of the clusters by extracting radio sources within $20'$ of clusters and trailing fields. The properties of these sources are summarized in Table 4. We also estimate their flux densities at AMiBA's operating frequency by simply assuming power law spectra of the form $S_\nu \propto \nu^\alpha$ with α the spectral index, assuming that source variability is not important.

In each field we find 20 – 30 objects in the NVSS and from 0-3 objects in the GB6 or PMN lists. Most of these sources are too faint to affect the AMiBA data, but two GB6 sources are bright enough to cause problems. The first is a source with $S_{4.85} = 192$ mJy

that lies $14'3$ from the center of the trail patch of A2261. The other has $S_{4.85} = 294$ mJy and lies $18'6$ from the center of A2390. However, the VLA calibrator catalog suggests that both sources have falling spectra above 8 GHz, with predicted 94 GHz flux densities of 130 ± 20 and 90 ± 20 mJy if the high-frequency spectra are power laws and variability is not important. Both sources lie beyond the half-power point of the AMiBA beam (at the 30% and 13% levels for offsets of $14'3$ and $18'6$, respectively; Wu et al. 2009). We take account of these sources by performing a simultaneous fit for the cluster SZE and the spectral indices of all sources with 4.85 GHz flux densities in Table 4 for these two clusters. We found spectral indices of -0.02 ± 0.13 (implying a 3 mm flux density $S = 203_{-67}^{+100}$ mJy) and 0.04 ± 0.03 (implying a 3 mm flux density $S = 328_{-198}^{+500}$ mJy) for the problem sources in the trail patch of A2261 and the main A2390 field, respectively. Although the sources are barely detected, we expect them to significantly affect the fitted value of I_0 .

None of the catalogued point sources is detected by AMiBA (at an rms sensitivity of 50 mJy) in the residual maps formed by subtracting the best-fit cluster SZE models from the visibility data. Therefore, we adopt a statistical method of estimating the contamination from the known point sources. This involves simultaneously estimating the spectral indices of known sources from 4.85 to 94 GHz and the value of I_0 for the cluster, as we did for A2261 and A2390. We do not use any prior on the spectral indices because the results are sensitive to the assumed distribution.

We cannot apply this method for the NVSS sources because the problem is generally underdetermined: there are too many NVSS sources per field. Instead we account for the contribution of NVSS sources using Monte Carlo simulations. In each of 500 runs, we pick a set of spectral indices for the sources from the *WMAP* distribution, predict the 94 GHz flux densities (forcing no source to exceed the GB6 or PMN limit), and estimate the visibilities. We then subtract these simulated visibilities from the AMiBA data, and re-fit the value of

I_0 and the spectral indices of the sources in the 4.85 GHz catalogs. We expect this to be an upper limit on the level of confusion from foreground and background radio sources not represented in the source surveys to date.

The effects of point sources on the value of I_0 are summarized in Table 3. We also show the effect of the offset induced by point sources in Figure 1 in the values marked by triangles. The value of I_0 increases by less than its random error in the four clusters without strong 4.85 GHz contaminating sources, but significant changes are seen for A2261 and A2390. In these cases, follow-up observations of the sources are highly desirable. The additional noise contributed by the population of point sources is, however, always considerably less than the noise from CMB anisotropies.

As pointed out by Giommi and Colafrancesco (2004), some unresolved sources with flat or inverted spectra may contaminate our SZ signal at 94 GHz. Further, these sources are mostly composed of the blazars. However, we conclude that the contribution of blazars to our observation is negligible by the analytical method as follows.

The visibility observed by point sources to each baseline is

$$\mathcal{V}(u, v) = \sum_i S_i(\nu) A(x_i, y_i) e^{-2\pi i(ux_i + vy_i)}, \quad (7)$$

where $S_i(\nu)$ is the flux density of the i th radio source. Assuming the radio sources are spatially distributed like a Poissonian random sample, the averaged visibility for each baseline is expected to be zero due to the two-patch subtraction technique. The rms fluctuation in each baseline then is

$$\begin{aligned} \langle \mathcal{V}^2(u, v) \rangle &= \frac{1}{\Omega} \langle \sum_i S_i^2(\nu) \rangle \int dx dy A^2(x, y) \\ &= \int_{S_{\min}}^{S_{\max}} dS S^2 \frac{dN(S)}{dS} \int d\alpha p(\alpha|S, \nu_0) \left(\frac{\nu}{\nu_0} \right)^2 \int dx dy A^2(x, y) \end{aligned} \quad (8)$$

where Ω is the normalized solid angle, S is the source flux density, and dN/dS is the differential source count as a function of flux. Typically, the differential source count is

described by a power law, i.e., $dN/dS = N_0 S^{-\gamma}$, where N_0 is a normalization parameter and γ is the power-law index. Since the differential source count of radio sources is well known only at low frequency, we are forced to rely on models to extend it to AMiBA’s operating frequency.

We use the Equation (8) to estimate the contribution from blazars on each baseline, and increase the resulting noise by $\sqrt{2}$ to take account of our two-patch subtraction technique. The source counts and the spectral energy distribution of blazars are well studied by Giommi and Colafrancesco (2004) and Giommi et al. (2006, 2009), and we adopt the values of N_0 and γ in Giommi et al. (2006) based on the combination of data from several radio and other surveys. We take the sources contributing in the AMiBA band to have the same distribution of spectral indices as those given by Giommi and Colafrancesco (2004), based on data between 5 and 150 GHz for a sample of 135 blazars from the NVSS-RASS 1 Jy survey (Giommi et al. 2002) and the 0.1 and 0.05 Jy points of the Deep X-Ray Radio Blazar Survey. We integrate Equation (8) from $S = 0$ to the flux density limits of GB6 (18 mJy) and PMN (40 mJy). We find that the rms contribution of blazars on each baseline is 13 mJy for A1689 and A2163 and 8.9 mJy for the other four clusters. These contributions are negligible compared with the SZE flux densities found for our cluster sample (about 150-300 mJy).

4. Discussion and Conclusion

The levels of contamination estimated in this paper are summarized in Table 3. Except for A2261, the dominant source of confusion is the primordial anisotropy of the CMB, which adds noise at the level of (13% – 50%) of the value of I_0 , exceeding the AMiBA system noise in every case. Galactic foreground emission is always negligible.

Known point sources affect the amplitudes of the SZE of the clusters by less than the combined system and CMB noises in each case except A2261, but ignoring the sources would systematically bias the estimates of I_0 since there are more radio sources towards the clusters than in the background fields. A2261 suffers particularly substantial contamination: both from the strong sources in the 4.85 GHz catalog (which cause a change $\Delta I_0 \sim -0.35 \times 10^5 \text{ Jy sr}^{-1}$) and from faint sources in the NVSS catalog (which cause a further effect $\Delta I_0 \sim -0.53 \times 10^5 \text{ Jy sr}^{-1}$).

Several other workers have reported on the discrete source environments of these clusters. Reese et al. (2002) report on radio sources at 28.5 and 30 GHz for A1689, A1995, A2163 and A2261. All of these sources are in NVSS, but none is bright enough at 5 GHz to appear in the GB6 or PMN catalogs: the brightest is a 10 mJy source in A2261. The VSA source-subtractor also reports on sources in A2142 (Lancaster et al. 2005): all are included in the NVSS catalog, and the contamination in the AMiBA data that they generate is small (less than 3% of I_0).

Tucci et al. (2008) have studied radio source spectra from 1.4 to 33 GHz. They found that, in general, the spectra are not well described by a single power law: the low-frequency spectra are usually steeper than the high-frequency spectra. Spectral index studies from 1.4 to 28.5 GHz (e.g., Coble et al. 2007) and 23 to 94 GHz (Wright et al. 2008) support this behavior. Our study, which extrapolated from 1.4 GHz (or 4.85 GHz) to 94 GHz using the *WMAP* spectral index distribution may therefore overestimate the contamination from radio sources.

Our best estimates of I_0 , taking contamination into account, are shown in the last column of Table 3, where we show the total uncertainty including the contributions from instrument noise, CMB, and point sources. The values given in this table are those used in the science analyses of our companion papers.

We acknowledge the extensive use we have made of data from the *WMAP* satellite, and thank Dr. L. Chiang for fruitful discussions on Galactic emission and the *WMAP* data. We also appreciate discussions with Drs. N. Aghanim and S. Matsushita on radio source properties. Support from the STFC for MB is acknowledged. This work is partially supported by the National Science Council of Taiwan under grants NSC97-2112-M-032-007-MY3 and NSC97-2112-M-001-020-MY3.

Table 3. Errors and Systematic Offsets in the Estimates of I_0 Caused by CMB Fluctuations and Radio Sources. The final estimate for I_0 includes these contributions and supersedes the value in Table 1.

Cluster	σ_{CMB} ($\times 10^5 \text{Jy sr}^{-1}$)	Source Offset ($\times 10^5 \text{Jy sr}^{-1}$)	Final I_0 ($\times 10^5 \text{Jy sr}^{-1}$)
A1689	0.53	-0.16 ± 0.17	-2.40 ± 0.71
A1995	1.02	$+0.28 \pm 0.27$	-3.10 ± 1.22
A2142	0.30	-0.24 ± 0.12	-2.40 ± 0.37
A2163	0.47	-0.01 ± 0.13	-3.16 ± 0.61
A2261	0.77	-0.88 ± 0.24	-2.34 ± 0.90
A2390	0.61	-0.51 ± 0.31	-2.93 ± 0.77

Table 4. Radio Sources in the Cluster Fields from 6 cm Catalogs.

Cluster	R.A. (J2000)	Decl. (J2000)	$S_{6\text{ cm}}^{\text{ a}}$ (mJy)	$S_{20\text{ cm}}^{\text{ b}}$ (mJy)	$S_{3\text{ mm}}^{\text{ c}}$ (mJy)	α	$\Delta\theta$ (arcmin)
A1995							
	14 52 50.8	57 46 58.0	28	25	36.0	0.08	16.0
	14 52 33.8	57 53 48.0	21	53	2.3	-0.75	9.3
	14 52 16.9	58 13 28.0	17	53	1.1	-0.91	11.5
	14 57 41.2	57 57 03.5	60	182	4.3	-0.89	12.7*
	14 57 56.3	57 44 47.1	56	81	23.0	-0.3	20.0*
A2142							
	15 58 13.0	27 16 22.4	39	107	3.5	-0.81	3.2
	15 58 34.9	27 30 45.0	21	17.4
	16 02 59.6	27 21 35.0	83	364	2.4	-1.19	6.2*
A2163							
	16 15 54.6	-6 08 44.0	42	5.3
	06 18 40.8	-6 17 18.0	56	10.0*
A2261							
	17 22 24.2	32 01 24.3	56	126	8.1	-0.65	6.3
	17 26 19.4	32 19 19.5	37	104	3.2	-0.82	15.2*
	17 26 20.5	32 01 26.0	29	11.7*
	17 26 35.3	32 13 30.0	192	126	522	0.34	14.3*
A2390							
	21 54 40.9	17 27 53.0	294	294	294	0	18.6
	21 57 05.4	17 51 15.0	81	270	4.6	-0.97	10.5*
	21 56 43.8	17 22 49.0	41	136	2.3	-0.93	19.1*

^aPMN and GB6 (Gregory et al. 1996; Griffith et al. 1995)

^bNVSS catalogs (Condon et. al. 1998)

^cExtrapolation to AMiBA frequency by power law

*Radio sources located in the trailing fields

REFERENCES

- Birkinshaw, M., 1999, *Phys. Rep.*, 310, 97
- Cavaliere, A., & Fusco-Femiano, R., 1976, *A&A.* 49, 137
- Chen, M.-T., et al., 2009, *ApJ*, 694, 1664
- Condon, J. J., Cotton, W. D., Greisen, E. W., Yin, Q. F., Perley, R. A., Taylor, G. B., & Broderick, J. J. 1998, *AJ*, 115, 1693
- Coble, K., Bonamente, M., Carlstrom, J. E., Dawson, K., Hasler, N., Holzappel, W., Joy, M., La Roque, S., Marrone, D. P., Reese, E. D. 2007, *AJ*, 134, 897
- Dunkley, J. et al., 2009, *ApJS*, 180, 306
- Giommi, P., Perri, M., Piranomonte, S., & Padovani, P. 2002c, in *Proc. International Workshop, Blazar Astrophysics with BeppoSAX and Other Observatories*, ed. P. Giommi, E. Massaro, & G. Palumbo (ASI SP; Frascati: ASI/ESA), 123
- Giommi, P., & Colafrancesco, S., 2004, *A&A*, 414, 7
- Giommi, P. et al. 2006, *A&A*, 445, 843
- Giommi, P. et al. 2009, *A&A*, 508, 107
- Gold B., et al., 2009, *ApJS*, 180, 265
- Gregory, P. C., Scott, W. K., Douglas, K., Condon, J. J., 1996, *ApJS*, 103, 427
- Griffith, M. R., Wright, A. E., Burke, B. F., Ekers, R. D., 1995, *ApJS*, 97, 347
- Ho, P.T.P., et al., 2009, *ApJ*, 694, 1610
- Huang, C., et al. 2009, *ApJ*. in press

Koch, P. M., et al. 2009a, ApJ, 694, 1670

Koch, P. M., et al. 2009b, ApJ, submitted (this issue)

Lancaster, K. et al., 2005, Mon. Not. R. Astron. Soc., 359, 16

Li, C.-T., et al., 2010, ApJ, in press

Liao, Yu-Wei et al., 2010, ApJ, 713, 584

Lin, K.Y. et al. 2009, ApJ, 694, 1629

Nishioka, H., et al., 2009, ApJ, 694, 1637

Reese, E. D., Carlstrom, J. E., Joy, M., Mohr, J., & Grego, L., 2002, ApJ, 581, 53

Molnar, S. et al. 2010, ApJ, submitted

Sunyaev, R. A., & Zel'dovich, Y. B., 1972, Comments Astrophys. Space Phys., 4, 173

Tegmark, M., Eisenstein, D. J., Hu, W., de Oliveira-Costa, A., 2000, ApJ, 530, 133

Tucci, M. et al., 2008, MNRAS, 386, 1729

Udomprasert, P. S., Mason, B. S., Readhead, A. C. S., and Pearson, T. J., 2004, ApJ, 615,
63

Umetsu, K. et al. 2009, ApJ, 694, 1643

Wright, E. L. et al. 2009, ApJS, 180, 283

Wu, J. H. P. et al., 2009, ApJ, 694, 1619